Faraday Discussions

Accepted Manuscript

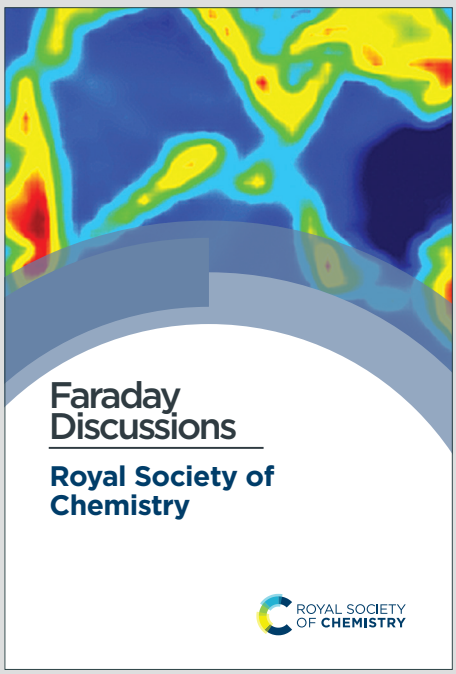

This article can be cited before page numbers have been issued, to do this please use: H. Braun, A. Remhof and C. Battaglia, *Faraday Discuss.*, 2026, DOI: 10.1039/D6FD00022C.

ROYAL SOCIETY OF CHEMISTRY

www.rsc.org/faraday_d

View Article Online
DOI: 10.1039/D6FD00022C

Understanding Solid Electrolyte Interphase Formation in Hydroborate-Based All-Solid-State Batteries

Hugo Braun [1,2], Arndt Remhof [1,2], Corsin Battaglia [1,3,4]

[1] Empa – Swiss Federal Laboratories for Materials Science and Technology, Dübendorf, Switzerland

[2] Institut für Anorganische und Analytische Chemie, Universität Freiburg, Germany

[3] Department of Information Technology and Electrical Engineering, ETH Zurich, Zürich, Switzerland

[4] Institute of Materials, School of Engineering, EPFL, Lausanne, Switzerland

Abstract

Hydroborate solid electrolytes are attracting increasing attention as alternatives to argyrodite electrolytes for all-solid-state lithium and sodium batteries. In this work, we first summarize recent progress in mixed-anion closo-hydroborate and closo-hydrocarborate electrolytes and derive criteria to select anion compositions that balance ionic conductivity, electrochemical stability, and interface compatibility. Building on a diffusion-limited interphase growth model, we quantitatively compare the interface resistance growth rate of $Li_3(CB_{11}H_{12})_2(CB_9H_{10})$ and Li_6PS_5Cl in contact with lithium metal, lithiated silicon, and delithiated NMC811 obtained by monitoring impedance as a function of time using electrochemical impedance spectroscopy. Despite its lower reductive stability, the hydroborate exhibits substantially slower interface resistance buildup in contact with lithium metal than the argyrodite, emphasizing that the transport properties of the solid electrolyte interphase, rather than the bulk electrolyte stability alone, govern long-term interfacial degradation. In contact with lithiated silicon, both electrolytes show markedly slower resistance growth, with the hydroborate showing higher stability than the argyrodite. In contact with delithiated NMC811, both electrolytes do not show any resistance growth at an open-circuit potential of 3.8 V vs Li/Li^+. At 4.1 V vs Li/Li^+, the hydroborate electrolyte shows resistance growth due to electrolyte oxidation, despite its higher oxidative stability compared to the argyrodite, which shows no resistance growth at this potential. The cell resistance is dominated by the interface resistance at the cathode highlighting the importance of protective coatings to prevent electrolyte oxidation. Our findings highlight closo-hydroborates and closo-carborates as promising electrolytes for high-energy solid-state lithium and sodium batteries and underline the critical importance of tailoring interphase composition and transport to unlock their full potential.

View Article Online
DOI: 10.1039/D6FD00022C

Introduction

All-solid-state batteries are widely regarded as a transformative technology for electric vehicles and aviation, promising higher energy density and superior safety. Expectations for their disruptive impact have therefore been immense, yet deployment in vehicles has lagged behind these ambitions, because the key bottlenecks, interfacial stability and chemo-mechanical robustness, have only recently begun to be addressed systematically.

Argyrodite electrolytes such as Li_6PS_5Cl are considered prime candidates for all-solid-state batteries due to their high ionic conductivity, sufficient deformability, and compatibility with scalable processing routes.[1, 2] Early demonstrations of solid-state batteries with argyrodites positioned them as benchmark materials against which emerging solid electrolytes can be compared.[3]

Hydroborates represent a promising, yet underexplored, class of electrolytes for all-solid-state batteries combining high ionic conductivity with a wide electrochemical stability window and favorable mechanical properties.[4] They typically possess low density comparable to liquid electrolytes enabling all-solid-state batteries with high specific energy.[5] Figure 1 compares the lithium-ion conductivity, the electrochemical stability window, and the density of the hydroborate $Li_3(CB_{11}H_{12})_2(CB_9H_{10})$ (green) and the argyrodite Li_6PS_5Cl (purple).

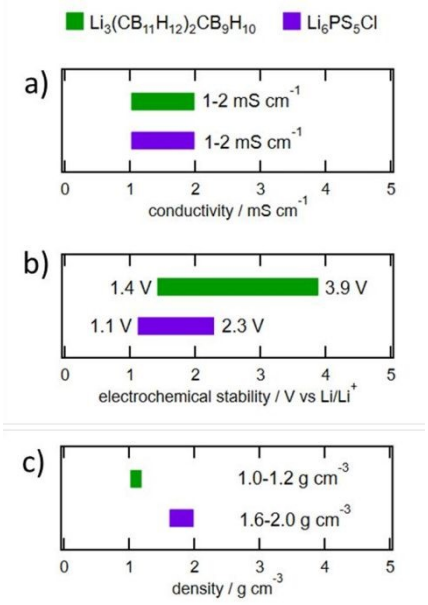

Figure 1: a) lithium-ion conductivity, b) electrochemical stability window, and (c) density of hydroborate $Li_3(CB_{11}H_{12})_2(CB_9H_{10})$ (green) and argyrodite Li_6PS_5Cl (purple) [1, 6-8]

Recent studies have successfully demonstrated the integration of hydroborates with 4 V-class intercalation cathode materials such as $LiNi_{0.8}Mn_{0.1}Co_{0.1}O_2$ (NMC811) [6] and $Na_3(VOPO_4)_2F$ [9] as positive electrodes enabling stable cycling to potentials up to 4.2 V vs. Li^+/Li or Na^+/Na.

View Article Online
DOI: 10.1039/D6FD00022C

Integration with low-voltage intercalation cathodes including TiS_2,[10-12] $LiFePO_4$,[13] $NaCrO_3$,[14, 15] and conversion cathodes such as sulfur[16] was also demonstrated.

On the anode side, both lithium metal and sodium metal have been integrated as negative electrodes in hydroborate-based solid-state batteries.[6, 9, 16, 17] While stable long-term cycling with minimal capacity fading was demonstrated for positive electrodes against In/Li and Sn/Na alloy anodes,[6, 15] cycle life against alkali metal anodes remains limited by their tendency to form dendrites. Recently, we showed that silicon-hydroborate nanocomposite electrodes enable stable cycling at high areal capacity of up to 3 mAh cm^{-2} with a remarkably slow interface resistance growth, demonstrating the feasibility of integrating silicon as a high-capacity negative conversion electrode in hydroborate-based solid-state batteries.[18]

In this study, we build on these recent developments to examine mixed-anion closo-hydroborate and closo-hydrocarborate electrolytes from a broader materials design perspective. We highlight structure–property relationships that help identify anion combinations that promote simultaneously high ionic conductivity and high interface stability. Furthermore, $Li_3(CB_{11}H_{12})_2(CB_9H_{10})$ is benchmarked quantitatively against Li_6PS_5Cl in terms of interface resistance growth rate in contact with lithium metal, lithiated silicon, and delithiated NMC811, to elucidate how hydroborates differ from argyrodites in their interfacial behavior and to pinpoint the most promising directions for further performance improvements.

Design principles for mixed-anion hydroborate and hydrocarborate electrolytes

Hydroborates are salts containing complex anions composed of covalently bonded boron and hydrogen atoms. Of particular interest for solid-state batteries are closo-hydroborates (or more specifically closo-hydridoborates), in which the boron atoms occupy the vertices of a polyhedron and are passivated by hydrogen atoms. The most stable anions are the doubly charged dodeca-hydroborate anion $B_{12}H_{12}^{-2}$ and the deca-hydroborate anion $B_{10}H_{10}^{-2}$ shown in Figure 2a and b. Related closo-hydrocarborates (or closo-carba-hydridoborates) have the same polyhedral structure, but with one of the boron atoms replaced by a carbon atom, resulting in the singly charged $CB_{11}H_{12}^{-1}$ and $CB_9H_{10}^{-1}$ anions shown in Figure 2c and d.

View Article Online
DOI: 10.1039/D6FD00022C

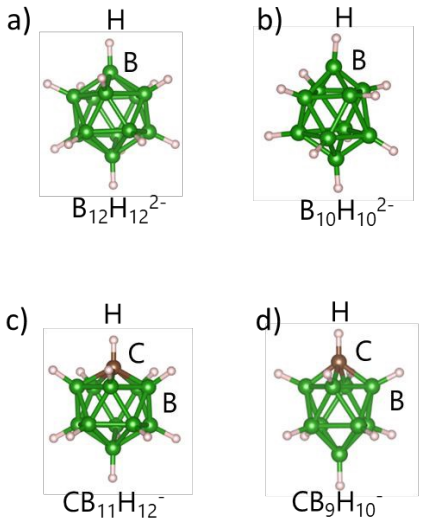

Figure 2: Atomic structure of the doubly charged hydroborate (a,b) and singly charged hydrocarborate (c,d) anions. $B_{12}H_{12}^{2-}$ is built from twelve symmetry-equivalent boron atoms, while $B_{10}H_{10}^{2-}$ has two distinct apical boron atoms and eight equatorial boron atoms. Consequently, the $CB_9H_{10}^{-}$ exists as two isomers, differing in the location of the carbon atom. The structure shown in (c) is the isomer with the carbon atom occupying an apical vertex.

At room temperature the corresponding lithium and sodium salts are in an ordered low-symmetry phase in which anions only possess librational degrees of freedom resulting in low cation conductivities < 10^{-5} S cm^{-1}.[19] Upon heating, the salts undergo a first-order phase transition to a high-symmetry phase in which the anions are orientationally disordered and rotate freely thereby promoting cation conductivities reaching values on the order of 10^{-1} S cm^{-1} at high temperature.[4, 20] The transition temperature increases in the following sequence $CB_9H_{10}^{-1}$, $CB_{11}H_{12}^{-1}$, $B_{10}H_{10}^{-2}$, $B_{12}H_{12}^{-2}$ showing a marked hysteresis between heating and cooling.[21] Ball milling was shown to be capable of suppressing this phase transition, resulting in cation conductivities of several 10^{-3} S cm^{-1} at room temperature.[22] There are, however, indications that the structural modifications induced by ball milling are not fully stable. Upon thermal annealing, the material gradually reverts toward its original structure accompanied by a corresponding decrease in conductivity.

Persistent cation conductivities of several 10^{-3} S cm^{-1} at room temperature can be achieved by stabilizing the high-symmetry phases via mixing of different anions into a solid solution. Combining $Li_2B_{12}H_{12}$ and $Li_2B_{10}H_{10}$ into $Li_4B_{12}H_{12}B_{10}H_{10}$ results in a cation conductivity of 4 10^{-4} S cm^{-1} [13] at room temperature which increases to 9 10^{-4} S cm^{-1} for $Na_4B_{12}H_{12}B_{10}H_{10}$.[17] The increase in conductivity when going from lithium to sodium is typical and can be explained with the larger size of the sodium cation resulting in lower electrostatic attraction between anions and cations. Electrostatic attraction between anions and cations can be further lowered by replacing doubly charged hydroborate anions by singly charged hydrocarborate anions. $Li_2CB_{11}H_{12}CB_9H_{10}$ exhibits a cation conductivity of 2 10^{-3} S cm^{-1} at room temperature[6] which increases to up to 7 10^{-2} S cm^{-1} for $Na_2CB_{11}H_{12}CB_9H_{10}$.[23] Mixtures of doubly charged hydroborate anions and singly

View Article Online
DOI: 10.1039/D6FD00022C

charged hydrocarborate anions such as $Na_3CB_{11}H_{12}B_{12}H_{12}$ were also explored resulting in a cation conductivity of 2 10^{-3} S cm^{-1}.[24]

Cation conductivity is an important criterion but equally important is the electrochemical stability. Oxidative stability increases in the following sequence $B_{10}H_{10}^{-2}$, $CB_9H_{10}^{-1}$, $B_{12}H_{12}^{-2}$, $CB_{11}H_{12}^{-1}$ [6, 13] resulting in the highest oxidative stability for $Li_3CB_{11}H_{12}B_{12}H_{12}$ and $Na_3CB_{11}H_{12}B_{12}H_{12}$. Oxidative stability can be promoted further kinetically, by moving away from an equimolar ratio using a combination of anions rich in the more stable anion such as $Li_3(CB_{11}H_{12})_2CB_{11}H_{12}$[6] and $Na_4(CB_{11}H_{12})_2B_{12}H_{12}$[9] enabling the integration of 4 V-class cathodes such as coated NMC811 and $Na_3(VOPO_4)_2F$. In the lithium case, the combination of two singly charged anions is preferred to maintain a lithium-ion conductivity at 1-2 10^{-3} S cm^{-1}, while the lower electrostatic attraction in the sodium case enables the use of a combination of a single charged anion with a doubly charged anion while maintaining a sodium-ion conductivity at 1-2 10^{-3} S cm^{-1}. An additional increase in oxidative stability is critical for high-voltage sodium-ion batteries due to the ~300 mV difference between the redox potentials of Li/Li^+ and Na/Na^+. Oxidation products forming in contact with a delihiated/desodiated cathode as predicted by density functional theory include oligomerized hydroborate anions, e.g., two or three $B_{12}H_{12}^{2-}$ oligomerized into a $Li_3B_{24}H_{23}$ dimer or $Li_4B_{36}H_{34}$ trimer, respectively. The dimer and trimer have a significantly higher predicted oxidative stability than the monomer ion, albeit with a lower reductive stability.[25] Note that in the case of $Li_3B_{24}H_{23}$ and $Li_4B_{36}H_{34}$, which are built from two and three hydrogen sharing $B_{12}H_{12}^{2-}$ anions, respectively, a fractional charge of 3/2 e and 4/3 e is contributed by each subunit of the dimer and trimer, respectively. Continuing this series, the charge thus reduces with (n+1)/n with n the number of anions reaching a charge of 1 e in the limit of infinite oligomer lengths. In principle, the resulting lowered electrostatic attraction favors higher cation conductivity. However, in parallel, oligomerization reduces the rotational degrees of freedom of the constituting anions, which is expected to be detrimental to cation conductivity. Anion mixing of oligomers with monomers offers a strategy to identify the optimum combination and indeed a cation conductivity of 1 mS cm^{-1} was demonstrated for the mixed-anion compound $Na_{18}B_{36}H_{34}(B_{12}H_{12})_7$,[26] composed of one trimer and seven monomers per formula unit.

The reductive stability increases in the following sequence $CB_9H_{10}^{-1}$, $CB_{11}H_{12}^{-1}$, $B_{10}H_{10}^{-2}$, $B_{12}H_{12}^{-2}$ [7] resulting in the highest reductive stability for equimolar mixtures with $Li_4B_{12}H_{12}B_{10}H_{10}$ and $Na_4B_{12}H_{12}B_{10}H_{10}$, which happen to be the most lithiated and sodiated binary mixed-anion compounds, respectively. However, while relatively stable cycling in contact with lithium and sodium metal anodes at current densities on the order of 0.1 mA cm^{-2} over extended periods of time is possible,[16, 17] time-dependent electrochemical impedance spectroscopy shows that these electrolytes get reduced, as shown previously for $Li_3(CB_{11}H_{12})_2CB_9H_{10}$.[7] In the spirit of the approach described above, compounds with higher reductive stability may be obtained kinetically, by using a combination of anions rich in the more stable anion, e.g., $Li_6(B_{12}H_{12})_2B_{10}H_{10}$. However, for this compound, the conductivity drops significantly compared to the equimolar mixture.[13] Reduction products predicted by density functional theory include LiB, LiH, and, if

View Article Online
DOI: 10.1039/D6FD00022C

hydrocarborates are involved, $LiBH_4$ as well as various $Li_xB_yC_z$ compounds.[7] Stability trends are summarized in Table 1.

Transition temperature	$CB_9H_{10}^{-1} < CB_{11}H_{12}^{-1} < B_{10}H_{10}^{-2} < B_{12}H_{12}^{-2}$
Oxidative stability	$B_{10}H_{10}^{-2} < CB_9H_{10}^{-1} < B_{12}H_{12}^{-2} < CB_{11}H_{12}^{-1}$
Reductive stability	$CB_9H_{10}^{-1} < CB_{11}H_{12}^{-1} < B_{10}H_{10}^{-2} < B_{12}H_{12}^{-2}$

Table 1: Qualitative ranking of different stability criteria for selected closo-hydroborate and closo-hydrocarborate anions including the transition temperature from the low-temperature low-symmetry phase to the high-temperature high-symmetry phase, the oxidative stability, and the reductive stability of the corresponding lithium and sodium salts.

Kinetics of solid electrolyte interphase growth

While it is important to consider the thermodynamic stability of solid electrolytes, the technologically relevant question is how rapidly the corresponding solid electrolyte interphases grow when in contact with electrodes. The chemical interface resistance growth is typically limited by diffusion such that interface resistance as measured by electrochemical impedance spectroscopy grows linearly with the square root of time. It is not a priori clear if the transport of lithium ions, or electrons, or the diffusion of lithium atoms is at the origin of the diffusion limitation.[27, 28] Figure 3a compares the interfacial resistance growth rate given in units of Ω cm^2 $h^{-0.5}$ of $Li_3(CB_{11}H_{12})_2CB_9H_{10}$ and Li_6PS_5Cl in contact with lithium metal. What is interesting here is that despite the 300 mV lower reductive stability of $Li_3(CB_{11}H_{12})_2CB_9H_{10}$ vs Li_6PS_5Cl (see Figure 1b), the hydroborate shows an almost 5x lower interface resistance growth rate than the argyrodite. The same trend is also observed in contact with delithiated silicon (Li_3Si), albeit with a 10x lower growth rate for both electrolytes as shown in Figure 3b indicating that the transport properties of the solid electrolyte interphase rather than the thermodynamic stability govern interface stability. The 10x lower growth rate in contact with Li_3Si compared to lithium metal is attributed to the lower chemical potential of lithium in Li_3Si, reducing the driving force for transport of lithium ions and electrons across the interphase, as detailed in the Wagner-type model for interphase growth.[27]

View Article Online
DOI: 10.1039/D6FD00022C

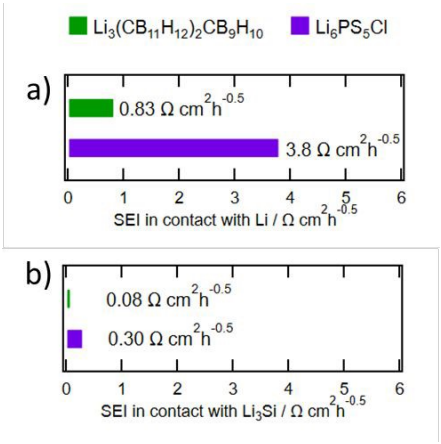

Figure 3: Interface resistance growth rate of hydroborate $Li_3(CB_{11}H_{12})_2(CB_9H_{10})$ (green) and argyrodite Li_6PS_5Cl (purple) in contact with a) lithium metal [7, 27] and b) lithiated silicon (Li_3Si) [18, 29]

When the electronic conductivity of the solid electrolyte interphase is negligible compared to the ionic conductivity, the interface resistance grows proportional to the square root of the electronic conductivity and the inverse of the ionic conductivity.[27] Both electrolytes possess roughly the same lithium-ion conductivity on the order of 1-2 10^{-3} S cm^{-1} (see Figure 1a). For the argyrodite-derived solid electrolyte interphase, the electronic conductivity was estimated at 3 10^{-10} S cm^{-1} and the ionic conductivity at 1.3 10^{-7} S cm^{-1} by synthesizing and characterizing solid electrolyte interphase material in bulk form.[30] In order to make a valid statement, the ex-situ synthesized solid electrolyte interphase material needs to have comparable composition and structure to the in-situ formed interphase material, which still needs to be determined in detail for hydroborates. Therefore, corresponding values for the hydroborate-derived solid electrolyte interphase have not yet been reported. A lower electronic conductivity and/or higher ionic conductivity of the hydroborate-derived solid electrolyte interphase compared to the argyrodite-derived solid electrolyte interphase would explain the slower interfacial resistance growth observed for the hydroborate in contact with lithium metal and lithiated silicon.

Figure 4 shows the corresponding interface resistance growth values for $Li_3(CB_{11}H_{12})_2CB_9H_{10}$ and Li_6PS_5Cl in contact with partially delithiated uncoated and coated NMC811, at an open-circuit potential of 4.1 V vs Li/Li^+ (after delithiation of 185 mAh g_{NMC}^{-1}). This potential is outside the stability window of both electrolytes (see again Figure 1b). However, only the hydroborate composite electrode shows interface resistance growth despite the higher oxidative stability, while the argyrodite composite electrode appears to offer sufficient interface passivation to prevent resistance growth at this potential. For the hydroborate, the interface resistance growth rate can be reduced from 25 to 11 Ω cm^2 $h^{-0.5}$ by applying a TiO_2-Li_2CO_3 coating on the NMC811 particles, indicating that the NMC811-hydroborate interface may be stabilized as well in the future by developing optimized protective coatings.

View Article Online
DOI: 10.1039/D6FD00022C

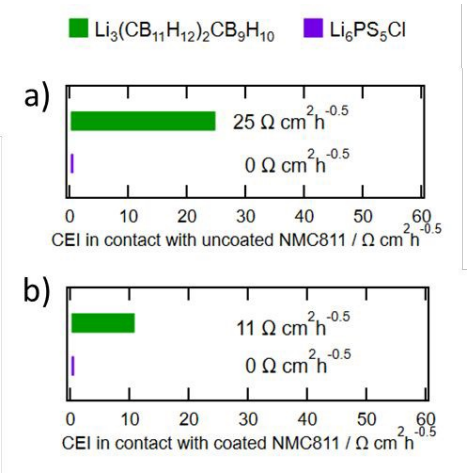

Figure 4: Interface resistance growth rate of hydroborate $Li_3(CB_{11}H_{12})_2(CB_9H_{10})$ (green) and argyrodite Li_6PS_5Cl (purple) in contact with partially delithiated (a) uncoated and (b) coated NMC811. The evolution of the impedance spectra over time and the corresponding fits using equivalent circuits models are provided in Figures S1-S10.

Notably, at an open-circuit potential of 3.8 V vs Li/Li^+ (after delithiation to 120 mAh g_{NMC}^{-1}), the hydroborate-NMC811 composite electrodes do not show any interface resistance growth (Figure S1), which is expected based on the oxidative stability limit of 3.9 V vs Li/Li^+ determined previously.[6]

Implications for cell design

Figure 5 summarizes the implications for solid-state battery design. Figures 5a and 5b illustrate the evolution of the interface resistance over a period of 365 days, extrapolating from the impedance measurements performed over ~100 hours. While diffusion may no longer be rate limiting at this timescale, the extrapolation is still useful to discuss long-term implications. The interface resistance does not typically extrapolate to zero at the beginning of the experiment due to an initial interface resistance which depends on the initial contact area, the applied stack pressure, temperature, and other parameters. The interface resistance of $Li_3(CB_{11}H_{12})_2CB_9H_{10}$ and Li_6PS_5Cl in contact with lithium metal reaches 100 and 360 Ω cm^2, respectively, after 365 days. In contact with lithiated silicon, the interface resistance reduces by a factor of 10. Meanwhile, the interface resistance of $Li_3(CB_{11}H_{12})_2CB_9H_{10}$ in contact with delithiated NMC811 reaches 950 Ω cm^2 after 365 days even with the protective coating. This highlights the need to develop improved coatings to prevent hydroborate electrolyte oxidation. While our measurements show negligible interface resistance growth for Li_6PS_5Cl in contact with delithiated NMC811, similar protective coatings are necessary for argyrodites as well, to enable operation of NMC811 electrodes at 4.2 V vs Li/Li^+ and above.[1]

View Article Online
DOI: 10.1039/D6FD00022C

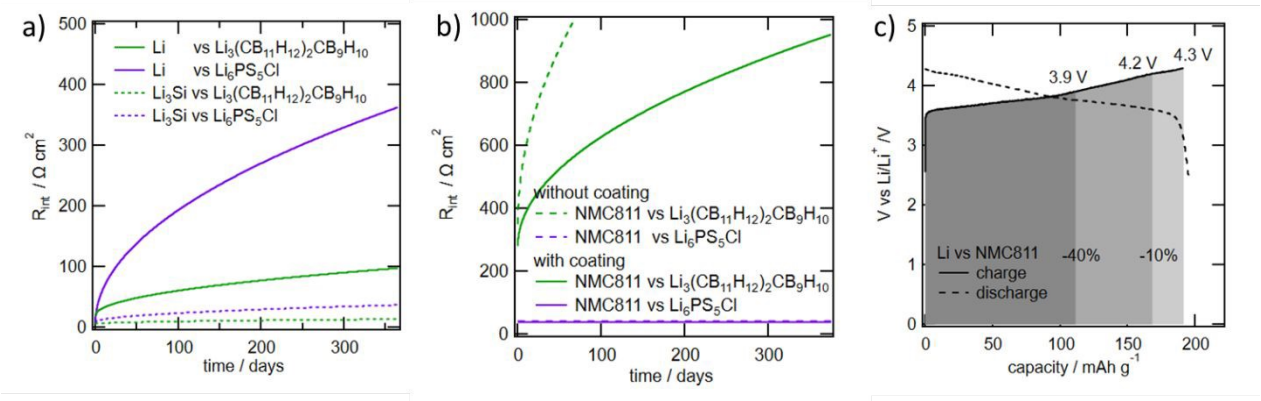

Figure 5: Time evolution of interface resistance calculated for hydroborate $Li_3(CB_{11}H_{12})_2(CB_9H_{10})$ (green) and argyrodite Li_6PS_5Cl (purple) in contact with (a) lithium metal and lithiated silicon, and (b) with delithiated uncoated and coated NMC811 at an open-circuit potential of 4.1 V vs Li/Li^+. (c) Voltage vs capacity curve of a NMC811 vs Li cell and impact of upper cut-off potential on maximum achievable discharge capacity.

When a cell is operated at 1 mA cm^{-2}, a bulk or interface resistance contribution of 100 Ω cm^2 causes a voltage drop of 100 mV. For a NMC811 vs Li cell cycled to an upper cut-off voltage of 4.3 V, this corresponds to a reduction in maximum achievable discharge capacity of about 10% as shown in Figure 5c and consequently also a 10% reduction in stored energy because the upper cut-off voltage is reached earlier leaving the upper state-of-charge window unused. If the cell resistance increases to 400 Ω cm^2, a corresponding voltage drop of 400 mV reduces the maximum achievable discharge capacity by about 40%, which is no longer acceptable. From this analysis, we consider that 100 Ω cm^2 represents a practical upper limit for the cell resistance, which should not be exceeded. The contribution of the interface resistance on the negative and positive electrode and the bulk resistance due to lithium-ion transport across the electrode(s) are in series and therefore add up to the overall cell resistance. For an electrolyte with a lithium-ion conductivity of 2 mS cm^{-1}, lithium-ion transport across a 100 µm thick composite electrode with an electrolyte to active electrode material volume ratio of 0.3 and a tortuosity of 1.5 accounts already for 25 Ω cm^2. For a NMC811/Li_6PS_5Cl/Li_3Si cell, the cathode and anode solid electrolyte interphase add another 40 Ω cm^2 each after 365 days. Summing these contributions results in a value slightly above 100 Ω cm^2. For a NMC811/$Li_3(CB_{11}H_{12})_2CB_9H_{10}$/$Li_3Si$ cell, the cathode electrolyte interphase dominates and contributes ~950 Ω cm^2 while the anode electrolyte interphase adds only 10 Ω cm^2. Our results highlight the importance of protective coatings for hydroborates to prevent electrolyte oxidation. Nevertheless, coated NMC811 embedded in $Li_3(CB_{11}H_{12})_2CB_9H_{10}$ cycled at C/2 to an upper cut-off potential of 4.2 V vs Li/Li^+ demonstrated already 70% capacity retention after 1000 cycles (167 days) and 54% after 2000 cycles (333 days) indicating that galvanostatic cycling conditions, for which the cell spends only 17% of its time above the oxidative stability limit, enable extended cycling stability.[6] Further studies are necessary to understand how the potentiostatic interface growth rates discussed here correlate with dis-/charge cycling results under different cycling

View Article Online
DOI: 10.1039/D6FD00022C

conditions, which are subject to additional impedance growth due to contact loss caused by volume changes and particle cracking of the active materials during cycling.

Conclusion

Our analysis confirms mixed-anion hydroborate electrolytes as strong contenders for all-solid-state batteries. Despite the lower reductive stability, $Li_3(CB_{11}H_{12})_2CB_9H_{10}$ forms interphases on the anode side that grow more slowly than those of Li_6PS_5Cl, in contact with both lithium metal and lithiated silicon, underscoring that the transport properties of the interphases, rather than bulk thermodynamics, control long-term stability. Conversely, despite the higher oxidative stability of $Li_3(CB_{11}H_{12})_2CB_9H_{10}$ compared to Li_6PS_5Cl and the ability to form oligomers upon oxidation with even higher oxidative stability, the interface resistance growth in contact with delithiated NMC811 is faster for hydroborates than for argyrodites, highlighting the importance of protective coatings to prevent electrolyte oxidation. Their superior interphase stability on the anode side positions closo-hydroborates as a serious competitor to argyrodites with the potential to enable long-lasting, high-energy all-solid-state batteries.

Supporting information

The evolution of the impedance spectra over time and the corresponding fits using equivalent circuits models are provided in Figures S1-S10. Materials preparation and cell assembly is described in detail in the Methods section.

References

1. C. Yu, F. Zhao, J. Luo, L. Zhang and X. Sun, *Nano Energy*, 2021, **83**, 105858.
2. B. D. Dandena, D.-S. Tsai, S.-H. Wu, W.-N. Su and B. J. Hwang, *EES Batteries*, 2025, **1**, 692–743.
3. S. Puls, E. Nazmutdinova, F. Kalyk, H. M. Woolley, J. F. Thomsen, Z. Cheng, A. Fauchier-Magnan, A. Gautam, M. Gockeln, S.-Y. Ham, M. T. Hasan, M.-G. Jeong, D. Hiraoka, J. S. Kim, T. Kutsch, B. Lelotte, P. Minnmann, V. Miß, K. Motohashi, D. L. Nelson, F. Ooms, F. Piccolo, C. Plank, M. Rosner, S. E. Sandoval, E. Schlautmann, R. Schuster, D. Spencer-Jolly, Y. Sun, B. S. Vishnugopi, R. Zhang, H. Zheng, P. Adelhelm, T. Brezesinski, P. G. Bruce, M. Danzer, M. El Kazzi, H. Gasteiger, K. B. Hatzell, A. Hayashi, F. Hippauf, J. Janek, Y. S. Jung, M. T. McDowell, Y. S. Meng, P. P. Mukherjee, S. Ohno, B. Roling, A. Sakuda, J. Schwenzel, X. Sun, C. Villevieille, M. Wagemaker, W. G. Zeier and N. M. Vargas-Barbosa, *Nature Energy*, 2024, **9**, 1310–1320.
4. L. Duchêne, A. Remhof, H. Hagemann and C. Battaglia, *Energy Storage Materials*, 2020, **25**, 782–794.
5. J. L. Hempel, S. Thapa, K. Kim, K. E. Kweon, B. C. Wood, Y. V. Sevryugina, R. Mohtadi, O. Tutusaus and Y.-T. Cheng, *Journal of Power Sources*, 2025, **641**, 236800.
6. H. Braun, R. Asakura, A. Remhof and C. Battaglia, *ACS Energy Letters*, 2024, **9**, 707–714.

View Article Online
DOI: 10.1039/D6FD00022C

7. H. Braun, Z. Łodziana, C. Battaglia and A. Remhof, *Journal of Materials Science: Materials in Energy*, 2026, **2**, 2.
8. T. K. Schwietert, V. A. Arszelewska, C. Wang, C. Yu, A. Vasileiadis, N. J. J. de Klerk, J. Hageman, T. Hupfer, I. Kerkamm, Y. Xu, E. van der Maas, E. M. Kelder, S. Ganapathy and M. Wagemaker, *Nature Materials*, 2020, **19**, 428–435.
9. R. Asakura, D. Reber, L. Duchêne, S. Payandeh, A. Remhof, H. Hagemann and C. Battaglia, *Energy & Environmental Science*, 2020, **13**, 5048–5058.
10. S. Payandeh, D. Rentsch, Z. Łodziana, R. Asakura, L. Bigler, R. Černý, C. Battaglia and A. Remhof, *Advanced Functional Materials*, 2021, **31**, 2010046.
11. S. Kim, K. Kisu, S. Takagi, H. Oguchi and S.-i. Orimo, *ACS Applied Energy Materials*, 2020, **3**, 4831–4839.
12. V. Gulino, M. Brighi, F. Murgia, P. Ngene, P. de Jongh, R. Černý and M. Baricco, *ACS Applied Energy Materials*, 2021, **4**, 1228–1236.
13. A. Garcia, G. Müller, R. Černý, D. Rentsch, R. Asakura, C. Battaglia and A. Remhof, *Journal of Materials Chemistry A*, 2023, **11**, 18996–19003.
14. L. Duchêne, R. S. Kühnel, E. Stilp, E. Cuervo Reyes, A. Remhof, H. Hagemann and C. Battaglia, *Energy & Environmental Science*, 2017, **10**, 2609–2615.
15. L. Duchêne, D. H. Kim, Y. B. Song, S. Jun, R. Moury, A. Remhof, H. Hagemann, Y. S. Jung and C. Battaglia, *Energy Storage Materials*, 2020, **26**, 543–549.
16. S. Kim, H. Oguchi, N. Toyama, T. Sato, S. Takagi, T. Otomo, D. Arunkumar, N. Kuwata, J. Kawamura and S.-i. Orimo, *Nature Communications*, 2019, **10**, 1081.
17. L. Duchêne, R. S. Kühnel, D. Rentsch, A. Remhof, H. Hagemann and C. Battaglia, *Chemical Communications*, 2017, **53**, 4195–4198.
18. H. Braun, C. Bürgel, E. Quérel, A. Remhof and C. Battaglia, *EES Batteries*, 2026, **2**, 597–608.
19. L. Duchêne, S. Lunghammer, T. Burankova, W.-C. Liao, J. P. Embs, C. Copéret, H. M. R. Wilkening, A. Remhof, H. Hagemann and C. Battaglia, *Chemistry of Materials*, 2019, **31**, 3449–3460.
20. W. S. Tang, A. Unemoto, W. Zhou, V. Stavila, M. Matsuo, H. Wu, S.-i. Orimo and T. J. Udovic, *Energy & Environmental Science*, 2015, **8**, 3637–3645.
21. R. Asakura, A. Remhof and C. Battaglia, in *Solid State Batteries Volume 1: Emerging Materials and Applications*, American Chemical Society, 2022, vol. 1413, ch. 14, pp. 353–393.
22. W. S. Tang, M. Matsuo, H. Wu, V. Stavila, W. Zhou, A. A. Talin, A. V. Soloninin, R. V. Skoryunov, O. A. Babanova, A. V. Skripov, A. Unemoto, S.-I. Orimo and T. J. Udovic, *Advanced Energy Materials*, 2016, **6**, 1502237.
23. W. S. Tang, K. Yoshida, A. V. Soloninin, R. V. Skoryunov, O. A. Babanova, A. V. Skripov, M. Dimitrievska, V. Stavila, S.-i. Orimo and T. J. Udovic, *ACS Energy Letters*, 2016, **1**, 659–664.
24. M. Brighi, F. Murgia, Z. Łodziana, P. Schouwink, A. Wołczyk and R. Cerny, *Journal of Power Sources*, 2018, **404**, 7–12.
25. R. Asakura, Z. Łodziana, R. Grissa, D. Rentsch, C. Battaglia and A. Remhof, *ACS Applied Energy Materials*, 2025, **8**, 9637–9645.
26. M. Jin, D. Xu, Z. Su, Z. He, X. Chen, R. Wu and Y. Guo, *ACS Energy Letters*, 2024, **9**, 1176–1183.
27. S. Wenzel, S. J. Sedlmaier, C. Dietrich, W. G. Zeier and J. Janek, *Solid State Ionics*, 2018, **318**, 102–112.

View Article Online
DOI: 10.1039/D6FD00022C

28. P. M. Attia, W. C. Chueh and S. J. Harris, *Journal of The Electrochemical Society*, 2020, **167**, 090535.
29. H. Huo, M. Jiang, Y. Bai, S. Ahmed, K. Volz, H. Hartmann, A. Henss, C. V. Singh, D. Raabe and J. Janek, *Nature Materials*, 2024, **23**, 543–551.
30. C. D. Alt, N. U. C. B. Müller, L. M. Riegger, B. Aktekin, P. Minnmann, K. Peppler and J. Janek, *Joule*, 2024, **8**, 2755–2776.

View Article Online
DOI: 10.1039/D6FD00022C

The data supporting this work are available from the corresponding author upon request.